Experimental analysis of the tensile property of FFF-printed elastomers

Xiang Lin[1], Phil Coates[2], Michael Hebda[2], Runguo Wang[3], Yonglai Lu[3], Liqun Zhang[3]

[1] *School of Chemistry and Biological Engineering, University of Science and Technology Beijing, 100083, Beijing, China*

[2] *Interdisciplinary Research Centre in Polymer Engineering, School of Engineering, Design, and Technology, University of Bradford, BD7 1DP, Bradford, West Yorkshire, United Kingdom*

[3] *College of Material Science and Engineering, Beijing University of Chemical Technology, 100029, Beijing, China*

Abstract:

Designing and manufacturing functional parts with enhanced mechanical property is a major goal of fused filament fabrication (FFF) for polymeric elastomers, which exhibits major advantages in producing such parts with a range of structures. But the unsatisfactory mechanical performance constrains greatly its real application and there is yet no consensus in the mechanical characterization of printed samples. This work takes the nozzle height as the considered factor and tests the tensile property of FFF-printed thermoplastic polyurethane (TPU). Rheological property of the TPU melt, represented here by die swell behavior and shear viscosity, were measured initially to obtain a preliminary assessment of the material suitability and an optimization of melt extrusion conditions for FFF processing. Then correlation between the cross-section profile of deposited bead and the tensile performance of printed sample were evaluated. Both the shape of deposited bead and the bonding strength of two adjacent beads are emphasized when explaining the measured tensile strength. The significance of molecular permeation efficiency at bead-bead interfaces, and bonding-releasing patterns between adjacent beads to the tensile failure of printed objects is discussed.

Keywords: Fused filament fabrication; Thermoplastic polyurethane; Nozzle height; Mechanical property.

1. Introduction

Additive manufacturing (AM) of polymers, also known as rapid prototyping manufacturing and 3D printing, has been well demonstrated with vigorous potential to reduce production cost and improve the design flexibility [1-5]. Since the concept of 3D printing was firstly proposed by Charles Hull in 1986, a series of AM

techniques have been developed for a range of materials [6, 7]. Thereinto, the most common method is called as fused filament fabrication (FFF). The feedstock filaments for FFF, composed of polymers (mainly thermoplastics [8]) or nanocomposites [9-12], are fed by a pair of gears. The melted filament is pressure-driven out from nozzle and then stacked layer by layer in accordance with predesigned patterns. This method is solvent free and suitable for processing expensive materials with large scale and hierarchical structure [13, 14].

A large number of internal interfaces and residual voids among adjacent beads might be formed during deposition. Such interfacial voids reduced the mechanical property of as-printed products. It is reported that the 3D printed products only exhibited ~10-73% of the strength as compared with the samples produced by injection molding or compression molding, and ~50% degree of mechanical anisotropy [15, 16].

However, standard tests to characterize the mechanical property for 3D printed objects are still required [17, 18]. Comparisons of the mechanical property exhibited by injection moulded and 3D-printed parts are conducted to provide a direct view of the mechanical weakness. Good mechanical property of 3D printed part was obtained by selecting the material [19], optimizing processing techniques [20] or tailoring the mesostructure of 3D printed samples. The key parameters include layer thickness [21], rastering angle [22], infill ratio (or 'air gap') [23], trajectory of the nozzle (or 'rastering pattern') [24] and building direction (or 'orientation') [25].

A particular difficulty for optimization of 3D printed products is the gap in understanding how to improve the mechanical property. Of significant interest within 3D printed parts is the bonding strength between adjacent beads, for enhanced understanding of fracture mechanisms. The bonding strength of two beads was reported to be largely dependent on the environment temperature and variations in convective conditions [26]. Then the bonding strength between adjacent beads was assessed based on the temperature degradation history. It was also reported that the best tensile property were obtained when the rastering orientation was aligned to the loading direction [23, 25, 27, 28]. Microvoids introduced during bead deposition were found to be large

contributors to the mechanical anisotropy and geometry errors in printed products [29-35].

Polymer elastomers, mainly in the form of powder, are commonly adopted for selective laser sintering. The mechanical performance of 3D printed products is dependent on the coalescence quality between adjacent particles. Critical factors in this process include particle size and shape [36], size distribution [37], processing parameters [38, 39] and materials nature physics [40]. However, little information is available on elastomeric filaments in FFF. A suitable material for FFF refers to low glass transition temperature T_g and high crystallization rate, but elastomers are generally amorphous and supplied above T_g. TPU filament provides high flexibility, strength and good resistance to abrasion and chemicals. This draws a great interest in printing soft TPU filaments for FFF fabrication, such as printing toy [41], medical parts with good mechanical performance [42] and strain sensor [43, 44]. However, few reports on printed elastomers focus on mechanical property [45-47].

Therefore, based on the 3D printed TPU, experimental work is presented here on the effect of nozzle height on tensile property. Analysis mainly focuses on the adhesion strength of bead deposition. Correlation between the tensile performance and the shape profile of deposited bead as well as packing morphology is emphasized when discussing the mechanical deterioration. Rheological property were measured to provide an initial assessment of material suitability for 3D printing and to evaluate the effect of die swell of the TPU melt. In order to explore the mechanical property dependence of as-printed products on key variables, tensile and delamination strength between two adjacent beads were investigated based on three laydown patterns. The mutual molecule diffusion promoting the interface formation was emphasized for the mechanical property of printed products. The tensile measurement in this work provides an insight of the mechanical dependence of printed TPU parts.

2. Experimental details

2.1 Materials

Commercial TPU filaments (Flex Pro98) with a diameter D_0 ~1.75 ± 0.05 mm were supplied by RS Components, Holland. This TPU material has a reported density of 1.16 g cm^{-3}, a melting temperature 225ºC, a high softening point of *ca.* 138ºC, a tensile stress at yield of ~50 MPa, a tensile modulus of 150 MPa and elongation at break of 450%.

2.2 Sample preparation and characterizations

The TPU filament was dried fully at 80ºC before printing. Rheological behavior of the TPU material were measured using capillary rheometer RH10 (Malvern, UK) and rotational rheometer MCR 301 (Anton paar, Austria) at the melt temperature of 215-240ºC. The as-received TPU filament was pelletized initially and hot compressed into round disks with the thickness of 1.5 mm. Particulate TPU and disk TPU were used for capillary shear and dynamic shear measurements, respectively. Capillary die with diameter D_c ~0.5 mm and aspect ratio L/D_c ~16 were employed and the zero die was matched. A desktop printer, Colido X3045 (China), was used and a common brass nozzle with inner diameter d ~0.4 mm and outer tip diameter D ~0.65 mm was adopted. The printer was controlled by Slic3r program with the following parameters: print speed ~70 mm s^{-1}, feeding rate 3.66 mm s^{-1}, infill density ~100% with rectilinear fill pattern of 90º angle and nozzle heights of 0.2, 0.3 and 0.4 mm. Scanning electron microscope (SEM) was adopted from Hitachi TM-3000 (Japan) to have an observation of the sample mesostructure. In order to remove the effect of perimeter layer on mechanical testing results, tensile specimens were cut from 3D printed flats using RAY-RAN (UK) in accordance with the ISO37-T4. The flat samples were printed with a designed thickness of 1.5 mm (Fig. 1). Tensile property was measured by means of Mach-1™ (Biomomentum Inc., Canada) with a tensile velocity of 0.5 mm s^{-1} at room temperature.

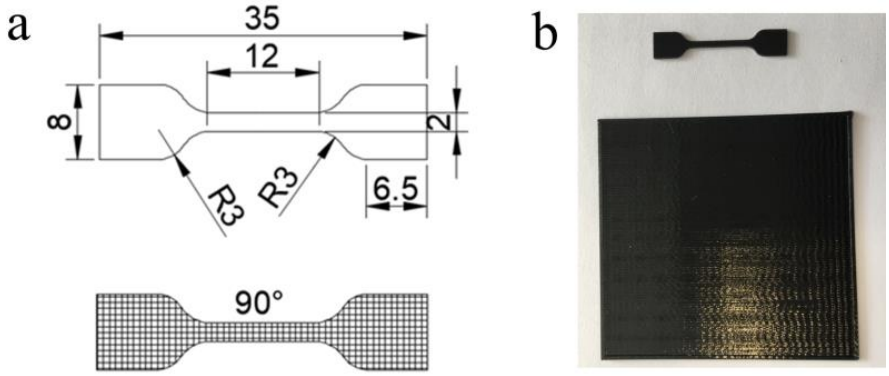

Fig. 1 Geometry of tensile sample (ISO 37-T4) (a) and the 3D printed plaque (75×75 mm) (b).

3. Results and discussions

3.1 Interaction between melt rheology and printing parameters

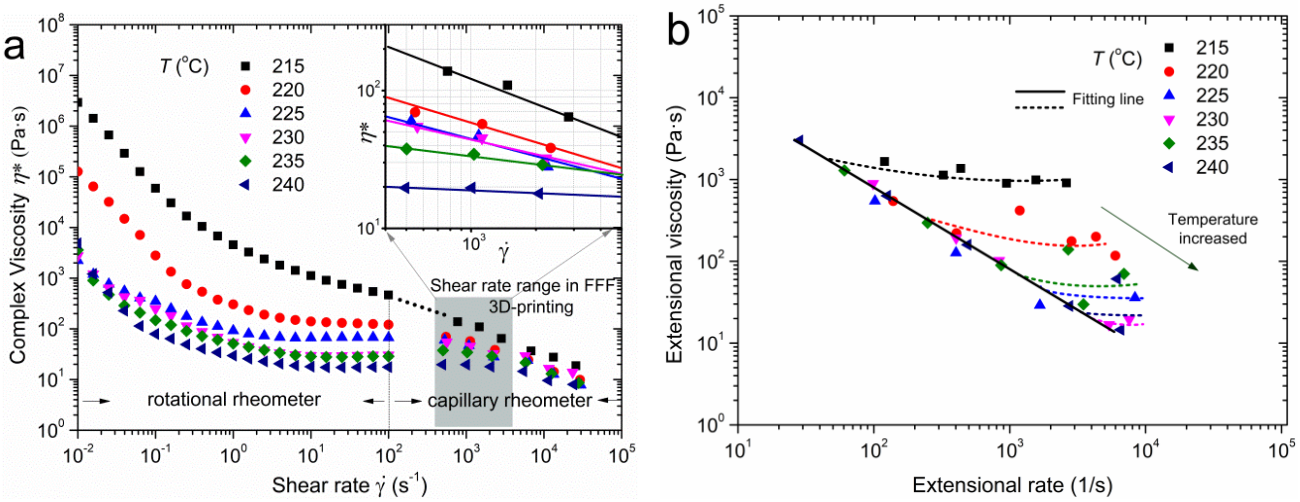

Fig. 2 Shear viscosity (a) and extensional viscosity (b) of the TPU melt.

During printing process, molten filament was extruded out of a hot nozzle and deposited onto a platform. The melt extrusion process essentially involves shear flow under a certain shear rate. It is well known that the flow behavior of the melt is largely dependent on its viscoelasticity, represented here by shear viscosity and die swell. The shear viscosity of molten TPU feedstock was measured by combining dynamic shear and capillary shear under 215-240ºC from 0.01 to 30, 000 s^{-1}, as shown in Fig. 2.

The melt volumetric flow rate from the nozzle was 4.0-17.5 mm^3 s^{-1} corresponding to filament feed gear revolution speed 3-13 rpm, resulting in the apparent shear rate at the nozzle exit from *ca.* 640 to *ca.* 2,800 s^{-1}. It should be noted that the melt flow rate should match the printing speed and it is controlled by slicing program.

The Bagley corrected shear rate within this feed revolution range is from *ca.* 730 to *ca.* 3, 200 s^{-1}. Results in Fig. 2 show that both temperature dependence of shear viscosity and shear-thinning behavior of the TPU melt are clearly seen. A higher melt temperature leading to a lower shear viscosity within the shear rate range is observed definitely. Extensional viscosity, based on the Cogswell principle, was calculated as one of the indices of elasticity, as shown in Fig. 2b. It can be seen that the extensional viscosity decreases with increasing extensional rate at the initial extensional rate stage and then reaches a plateau value. However, the observed dependence of extensional viscosity on temperature indicates that to raise the melt temperature could decrease melt elasticity and to reduce die swell.

During the rastering process, the TPU melt was pressure-driven out of the nozzle tip, incurring die swell. The die swell was observed to affect layer height, infill percentage, surface roughness and mechanical performance of the printed products. The diameter of the extrudate $D_{\text{extrudate}}$ (normally cylindrical shape) demonstrated with a swell ratio δ. The die swell ratio was calculated by:

$$\delta = D_{\text{extrudate}} / D_{\text{nozzle exit}}. \quad (1)$$

The extrudate diameter $D_{\text{extrudate}}$ was measured at the location where the die swell was fully developed. Interestingly, constant δ is revealed with the increasing feed rate (see Fig. 3a). The swell ratio δ is presented to be a linear function of nozzle temperature T (Fig. 3b). The melt flow rate and nozzle exit shear rate are linearly determined by filament feed gear revolution speed (Fig. A.1). At 235ºC nozzle temperature, the diameter of the extruded bead was similar to the nozzle diameter ($\delta \approx 1.083$), and at 240ºC negative expansion was observed ($\delta \approx 0.976 < 1$). This effect is due to the reduced elasticity of TPU melt. Extruded beads with $\delta \sim 1$ are preferred because they are observed to maintain their shape during rastering, which would allow better control of the 3D printed parts.

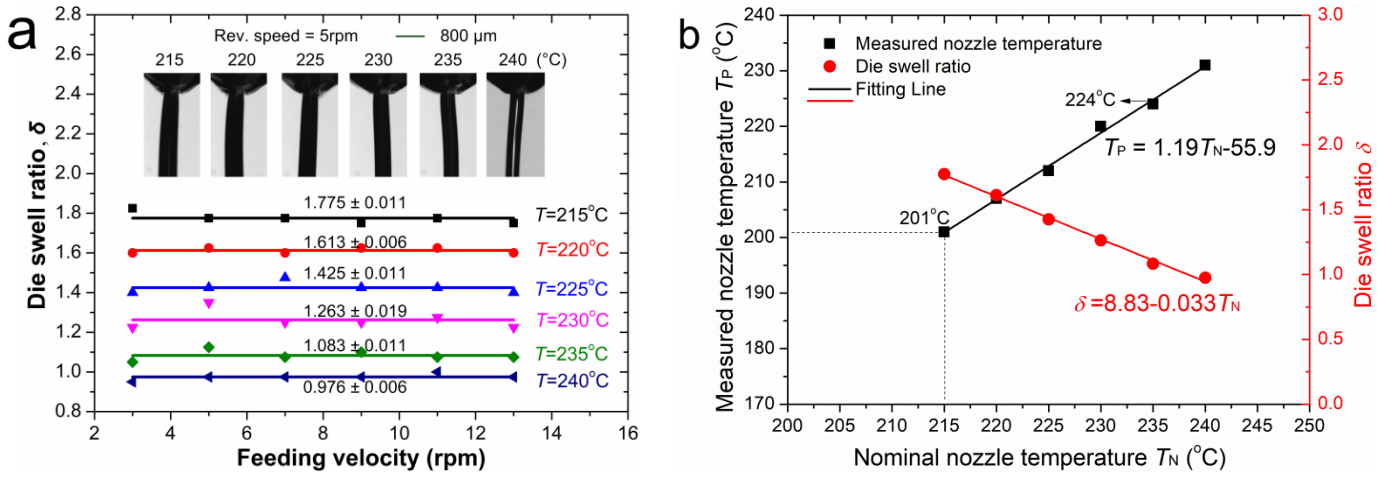

Fig. 3 Die swell ratio δ under varied feed velocities and set temperatures (a); actual nozzle temperature and the dependence of δ on T_N (b).

Consequently, the nozzle temperature was set at 235ºC. However, large difference was observed (Fig. 3b) between the measured nozzle temperatures (T_P) and the set temperatures (T_N) by inserting a thermocouple inside the nozzle channel (see Fig. A.2). For example, a measured temperature of 224ºC was obtained instead of the set value 235ºC. This suggested that the TPU melt could be deposited at ~ 224ºC during rastering. Thus, the referenced melt shear viscosity at the nominal nozzle temperature 235ºC should be selected from the measured capillary shear viscosity at the temperature of 224ºC, i.e., η^*~ *ca.* 52-26 Pa·s corresponding to the corrected shear rate of *ca.* 730-3, 200 s^{-1}. In addition, the zero shear viscosity η_0 of TPU melt at the set nozzle temperature 235ºC approached to *ca.* 2, 230 Pa·s which was obtained at the actual melt temperature 224ºC, which was provided by the dynamic shear at 0.01 s^{-1}.

3.2 Mechanical dependence on bead packing geometry

Raster orientation, which is controlled by toggling between two angles from one layer to the next, is usually emphasized when discussing the mechanical property of 3D-printed objects. For example, parallel construction (-0º/0º) can be achieved by rastering melted polymer lines in the same direction. According to reference [29, 47], the parallel layers (raster angle = 0º) provided the best mechanical performance and the highest degree of anisotropy. Advincula *et al.* [14] characterized the mechanical property of 3D-printed

products and they found that anisotropic mechanical property were commonly observed and the best tensile performance were obtained in the direction of alignment of the beads, but this leads to significant anisotropy in the product. In this work, a rastering angle of 90º was selected in order to reduce mechanical anisotropy of the printed sheets from which ISO 37-T4 tensile samples were cut. Nozzle height has been found to be critical to control the geometry of deposited beads, which influences packing density. When a bead is extruded out of the nozzle exit and deposited on the bed or previous layer, the bead will be squeezed if the nozzle height h is less than the bead diameter. The effect of nozzle height h on packing geometry was measured by SEM (Fig. 4).

If the nozzle height is larger than the extrudate diameter and the printing speed is higher than the melt extrusion velocity, it is likely that control of bead geometry will be lost during the rastering process. Figure 4a shows that the deposited beads were packed densely for h=0.2 mm, giving rising to a few minor voids. For h=0.3 and 0.4 mm non-contacted fused beads were observed, leading to high porosity (Fig. 4b, 4c respectively). This lead to more serious mechanical deterioration, as such unbonded beads will fail to transfer external loading.

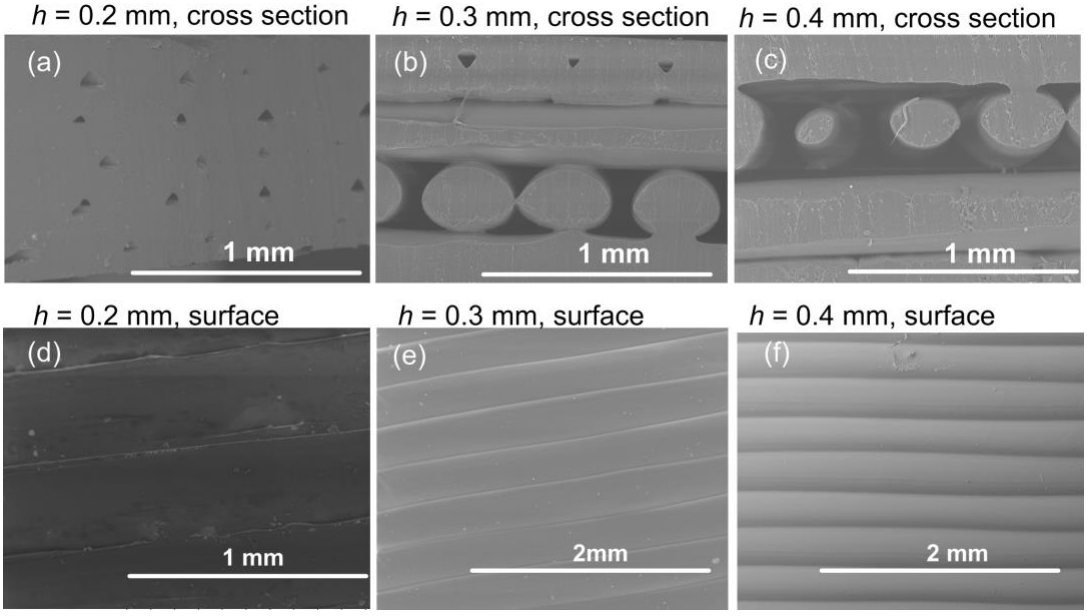

Fig.4 Effects of nozzle height on the geometry of cross-section (a)-(c) and surface features (d)-(f).

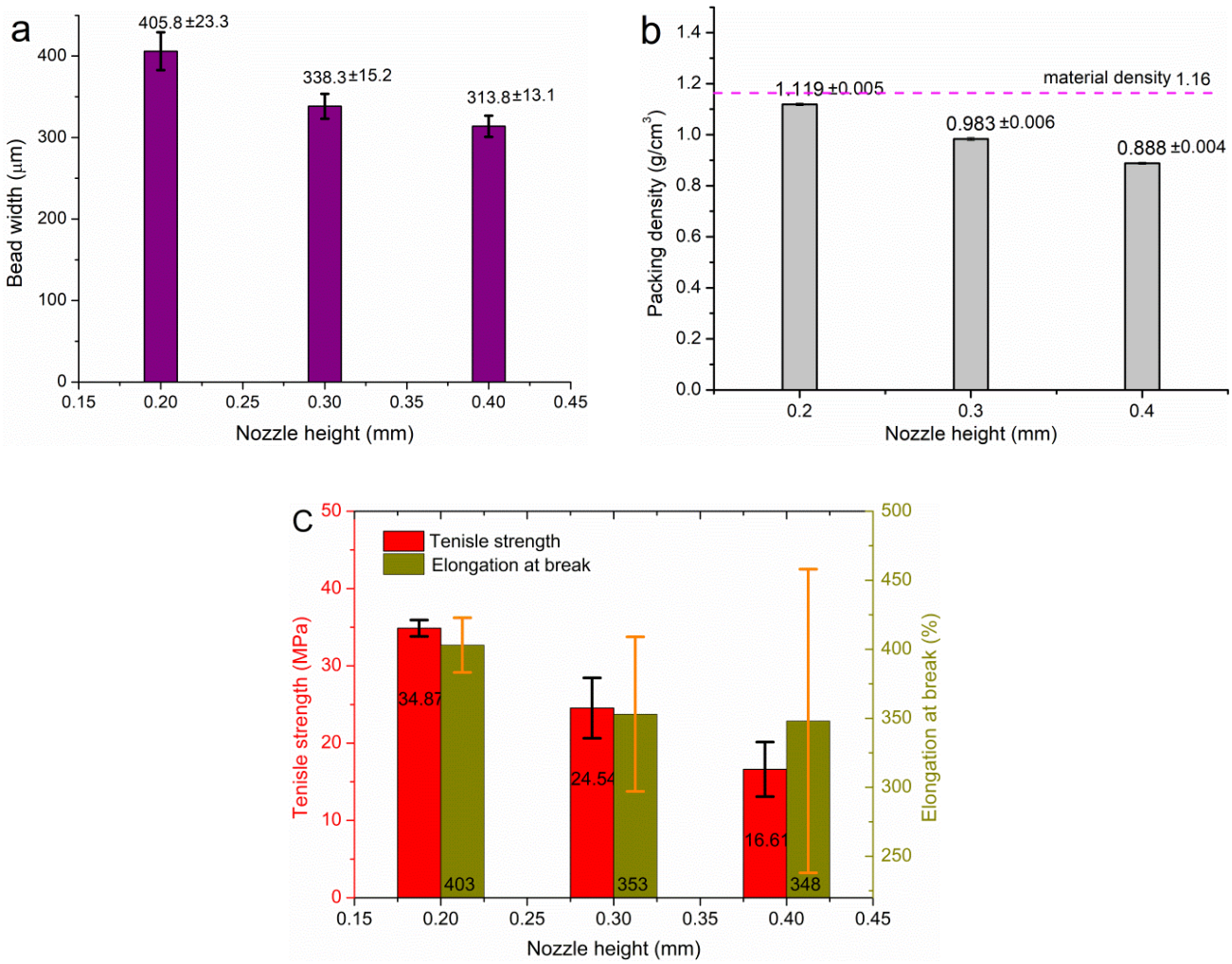

Fig. 5 Bead width (a), packing density (b) and yield tensile property (c) of 3D printed TPU samples.

Figure 5a shows the width of the beads illustrated in Figs. 4d, e &f versus nozzle height. It can be seen that the bead width decreases with increasing *h*, and the width of the beads deposited for *h*=0.3 and 0.4 mm are lower than the nozzle exit diameter (~ 0.4 mm), i.e. there will be more free surface flow of the melt (i.e. less control of bead geometry) under these conditions. Also when the nozzle traverse speed is higher than the melt extrusion velocity, the melt extrudate will be stretched along the rastering direction. In this case, the adjacent parallel beads separate from each other with a visible gap between them, leading to a decrease of packing density (Fig. 5b), and a consequent drop in tensile strength (Fig. 5c). We note that the generated voids could also have a significant negative impact on the fatigue property of printed parts. The lowest packing density ~0.888 g·cm^{-3} (~76.6% of material initial density) is observed in the samples printed at *h*=0.4 mm, while the highest packing density ~1.119 g·cm^{-3} (~96.5% of material density) corresponds to the samples printed at

h=0.2 mm. The samples deposited at h=0.2 mm demonstrate a tensile strength of ~34.9 MPa and an elongation at break of ~403%, which were 69.7% of tensile strength and 89.6% of elongation at break of the TPU bulk material, respectively. The tensile property of the as-printed TPU for h=0.2 mm show good retention of material strength but lower elongation at break.

3.3 Cross-sectional geometry of deposited beads

The cross-sectional geometry of deposited beads is critical for tailoring interfacial bonding quality and mutual molecular diffusion during the FFF process. The temperature gradient of the melting region and the feeding velocity are crucial to melting the filament fully and feeding it steadily. The significance of extrusion stability and continuity on the control of bead shape has been emphasized to obtain better control of porosity and mechanical property in previous studies [49-51].

Figure 6a illustrates the effect of nozzle height h on bead shape profile. When h is lower than the bead diameter and the nozzle traverse velocity is lower than the melt extrusion velocity, the deposited beads will be squeezed by the nozzle tip with a compression stress, σ_c. In this case, the actual width W of the bead will be enlarged. Such squeezing effect further contributes to edge overlapping of adjacent beads. The squeezing stress σ_c derives from the normal compression force F_N which is related to the viscosity and flow rate of the extruded melts [49, 51]. Figs. 6b&c present the single deposited bead shape of two adjacent beads which were deposited at the same nozzle temperature, nozzle traverse velocity and feeding rate. The feeding rate was set as ~ 0.0567 mm filament feeding length per unit nozzle moving length ~1.0 mm (assuming steady, continuous melt extrusion). The adjoining beads show varied outcomes indicating that the bead deposition does not accurately follow nozzle traverse across the printer bed. Distorted bead lines are shown in Figure 6c. An elongated rectangular cross section with rounded edges is observed for h ~ 0.2 mm while a more circular cross section is revealed by increasing h. However, the actual layer thickness is still far from the set value of h. A well bonded interfacial layer will enhance mechanical performance of the printed product, while poor adhesion

could lead to layer delamination under external loading. The variation in width and thickness of deposited beads are shown in Fig. 6d. The bead thickness increases and bead width decreases with the increase of nozzle height *h*. The average bead thicknesses of beads are 0.137, 0.245 and 0.266 mm for the beads deposited at 0.2, 0.3 and 0.4 mm nozzle height, respectively. The observed thicknesses of the tested beads were always lower than the nozzle height under which the beads were deposited. The spread in the *W* outweighed *h* in all tested samples for TPU which implies a different set of material characteristics when compared with PLA and ABS, commonly used FFF materials, from the experiments in [51]. More irregular shapes were observed for the TPU beads without a significant deformation recovery.

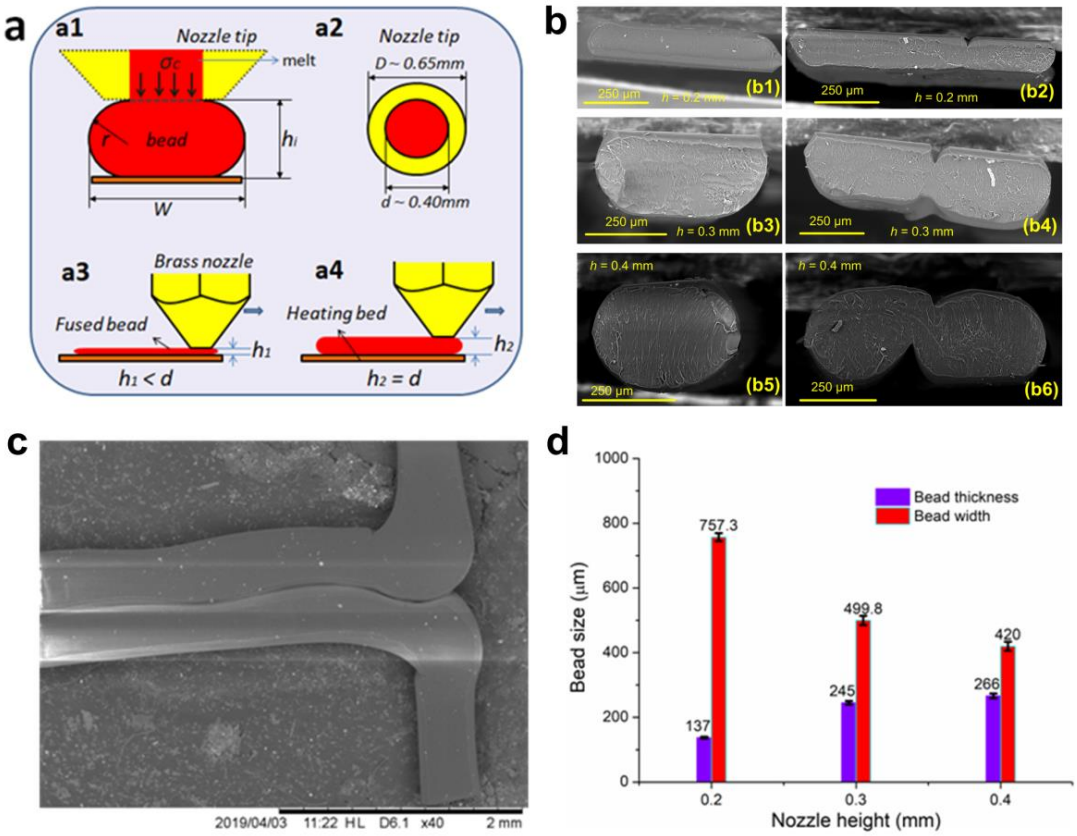

Fig. 6 Schematics of die swell and squeezing effect (a), bead geometry of cross-section (b), bead distortion (c) and bead width and thickness (d).

3.4 Bonding strength between two adjacent beads

Beads which are not parallel to the direction of externally imposed force on a printed product could be subjected to a component of the force transverse to the bead, potentially causing delamination of the beads.

Therefore, the deposited beads of a tensile specimen could be subjected to tensile force and delamination force simultaneously. Two kinds of bond delamination have been explored: bead to neighbouring bead, and bead to a substrate layer of beads. Three lay-down patterns were used to evaluate bead delamination, as shown in Figs. 7a-c. Two adjacent beads bonded with the deposition patterns were printed for tensile measurement.

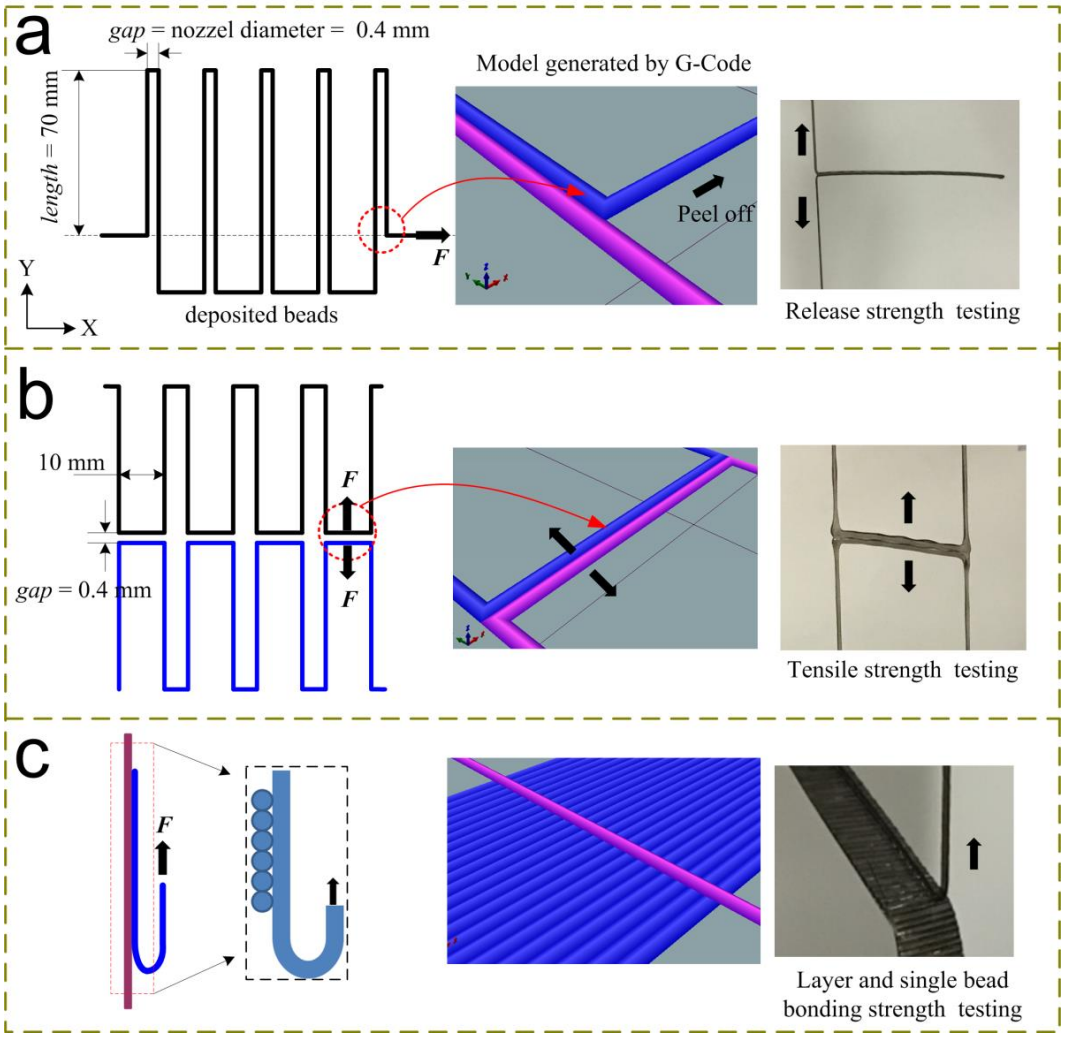

Fig. 7 Schematics of the bead deposition patterns: (a) bead-bead tensile, (b) bead-bead release and (c) bead-layer.

Figure 8 shows both release and tensile force of the bonded beads corresponding to the patterns in Figs. 7a & 7b, respectively. It can be seen that both the release force and the tensile force decrease with the increase of nozzle height due to the varied interfacial features (Fig. 6b). The adjacent beads deposited at lower nozzle heights promoted molecular diffusion due to the increase of interfacial area. The delamination and tensile

behaviour of individual beads are shown in supplementary Figs. A.3 & A.4. The delamination force of the bonded beads fluctuates during the tensile test, demonstrating sinusoidal variation with strain. The peak value is regarded as the critical peeling (delamination) force between two adjacent beads, i.e. bonding force, as shown in Fig. 8.

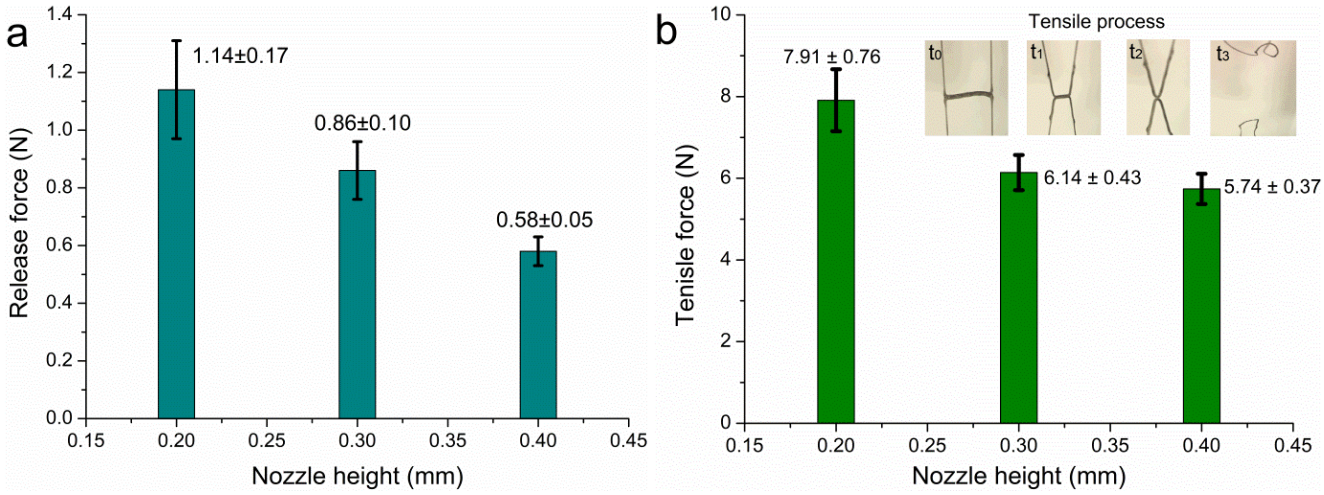

Fig. 8 The delamination force of two adjacent beads corresponding to Figs. 8a & b.

For the pattern of a single bead sticking to a substrate layer (see Fig. 7c), the release force was also measured and the release behavior was found to be more irregular, as shown in Fig. 9. When nozzle height h was set at 0.2 and 0.3 mm, the deposited bead was squeezed and then stacked upon the substrate layer. But for $h \sim 0.4$ mm, such squeezing effect was less significant. This reduces the bonding strength between the single bead and the layer. For samples built at $h \sim 0.2$ and 0.3 mm, the onset of the release behaviour happens at the point where the bonding interface begins (Figs. 9a&b). For $h \sim 0.4$ mm, however, a fluctuating release force was observed. This is because the deposited bead is not fully bonded with the layer surface, i.e. in partially contact.

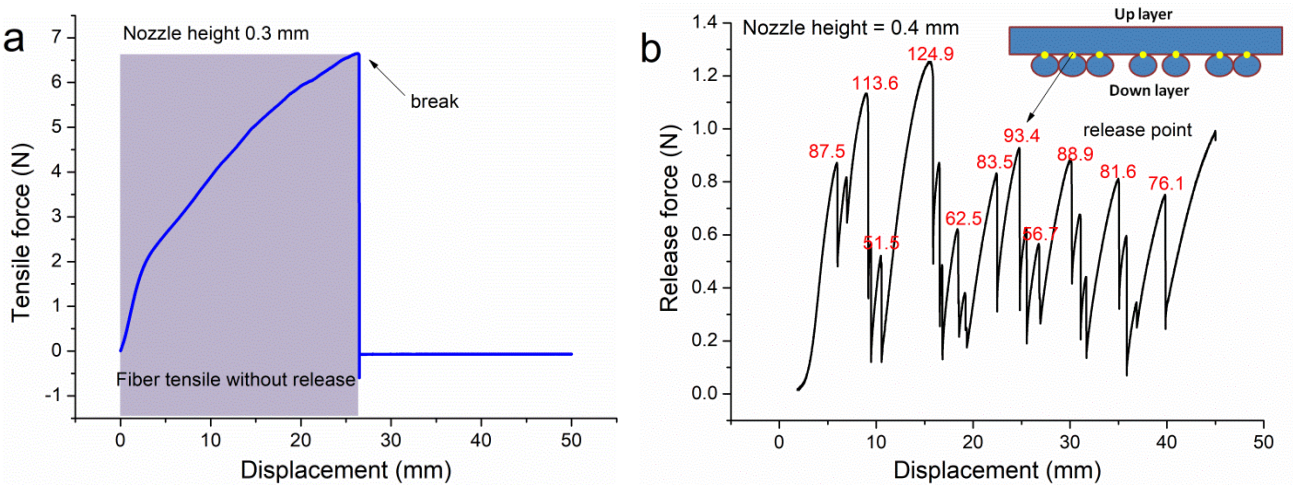

Fig.9 Release behaviours of a bead stacking on succeeded layer at *h*=0.3 mm (a) and *h*=0.4 mm (b).

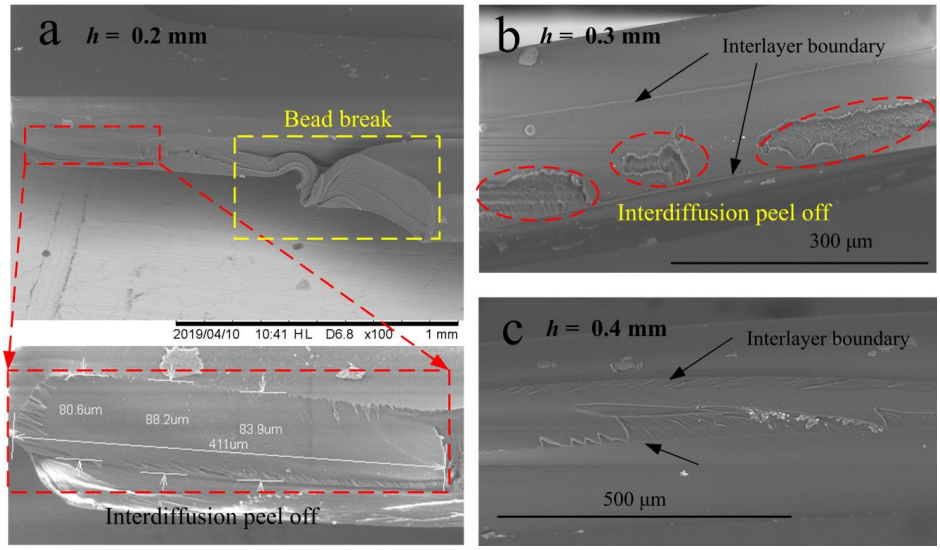

Fig. 10 Delamination between adjacent beads printed at: (a) *h*=0.2 mm, (b) *h*=0.3 mm and (c) *h*=0.4 mm.

Figure 10 illustrates the typical delamination features of bonded beads after tensile testing. Interfacial diffusion between two adjacent beads is observed clearly for all the samples deposited under varied nozzle heights. The bonding quality of two adjacent beads shows a decreased trend with the increase of *h*. For samples deposited at *h*= 0.2 mm, fracture failure of the bead is observed after being delaminated for ~ 411μm (the width of the interface is ~80-88μm). However at *h*= 0.4 mm only interfacial delamination is observed, due to a lower degree of molecular diffusion. The crack-tip failure behaviour shown in Fig. 10a is similar to elastic-plastic fracture mechanic characteristics [52], indicating a high quality of interfacial bonding at *h*= 0.2 mm.

3.5 Discussion of the effect of molecular diffusion across interface on bonding strength

It is recognised that all the factors promoting the mutual diffusion process at bead interfaces can enhance the mechanical property of printed products. Shmueli *et al.* [53] emphasized the effect of temperature profile during printing on the structure/property of samples. The mutual molecular diffusion between adjacent beads was found to be a function of sintering time and temperature.

The model proposed by Pokluda *et al.* [54] is used to describe the diffusion process, as shown in Eq. (2).

$$\frac{d\theta}{dt} = \frac{\Gamma}{d_0 \mu} \frac{2^{\frac{-5}{3}} \cos\theta \sin\theta (2-\cos\theta)^{\frac{1}{3}}}{(1-\cos\theta)(1+\cos\theta)^{\frac{1}{3}}}, \qquad (2)$$

where $\theta = \sin^{-1} y/r$ represents the diffusion degree by ratio of the formed neck height $2y$ to bead diameter $d=2r$ (see Fig. 6a), Γ is surface tension, d_0 is initial bead diameter, μ is melt viscosity and t is sintering time. The ideal value of y is expected to approach to r. During this diffusion process after depositing, the temperature T is coupled with time t which can be described by the energy balance equation as

$$\rho C A v \frac{\partial T}{\partial x} = A \frac{\partial\left(k \frac{\partial T}{\partial x}\right)}{\partial x} - hP\left(T - T_\infty\right), \qquad (3)$$

where ρ is material density, C is specific heat, A is bead cross section area, v is printing velocity, h is thermal conductivity (including convection) with air and foundation, T_∞ is equilibrium temperature and P is perimeter length.

In a 3D printing process, the interface growth occurs between two adjacent beads of which one is assumed to be in the melt state and the other is solid phase (previously deposited). The squeezing behaviour, on the one hand, changes the cross-section outline of the deposited beads, and on the other hand, results in difference of the interfacial layer contact area and original neck formation. After the TPU melt is deposited onto the bed, the melt temperature (~224ºC) will typically reduce to the bed temperature in less than 2.5 seconds [53]. If the TPU melt is deposited onto a substrate layer, however, the previously deposited beads could be reheated

rapidly by the hot melt and then achieve an equilibrium thermal state. Therefore, the temperature-driven diffusion process can be assumed to be mainly promoted by the hot melt [26]. In this case, Eq. (3) then can be rewritten as

$$m_1 \frac{\partial T}{\partial x} = \frac{\partial\left(k \frac{\partial T}{\partial x}\right)}{\partial x} - \frac{P}{A} m_2, \qquad (4)$$

where m_1 and m_2 are constants related to material properties and printing parameters, e.g. the printing speed and the envelope temperature. When the printing speed and nozzle temperature are constant, given the initial (depositing) and infinite (envelope) temperatures, the bead cooling process is expressed in terms of bead geometry, i.e. A and P.

According to Arrhenius law, the deposited TPU beads should have the identical activation energy ΔE under the same envelope temperature and therefore the molecular chains behave identical diffusion ability in interface bonding process. Owing to the same material of the adjacent beads and the identical printing parameters, factors of specific heat capacity, heat transfer efficiency, surface (tension) energy and heat conductivity of material are identical. The self diffusion coefficient D_s obeys the Arrhenius law [55]:

$$D_s(T) = D_0 \exp(-Q / RT) \qquad (5)$$

where Q is the activation energy, D_0 is a pressure-dependent constant, R is Molar gas constant and T is bulk temperature. Higher heat flux could be obtained by increasing the heat conduction area which is related to the interfacial area, i.e. contacting area between two beads. The diffusion behaviour of the adjacent beads could be equivalent during the interface formation. The interfacial bonding strength, therefore, is then dominated by the contact surface area. This increase of contact area not only promotes the thermal transmission but also enhances the molecular chains diffusion (Fig. 11). The heat energy of the most recently deposited bead (red) transfers to the lower cooled bead (blue) and it therefore reheats the cooled bead. The interfacial surface is then expanded, which is helpful to enhance the mutual diffusion. When the bead temperature decreases to the

ambient or substrate temperature, the development of interfacial layer terminates, achieving an equilibrium state.

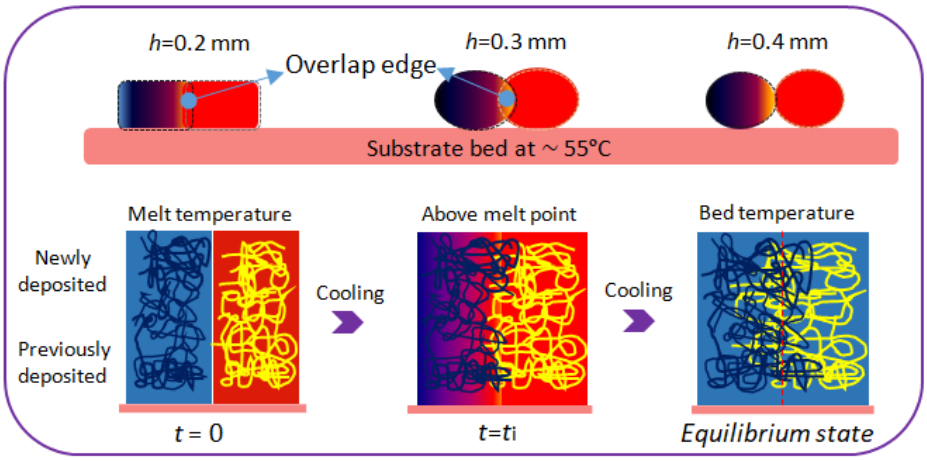

Fig. 11 Schematic diagram of diffusion process between a hot bead and a cool bead.

4. Conclusions

This work provides an experimental approach to elucidate the mechanical dependence of 3D printed TPU on printing parameters, taking the nozzle height as an example. Within the shear rate range in FFF processing, the die swell ratio of deposited bead strand is found to be dominated by nozzle (hence polymer melt) temperature, and changes linearly with the nozzle temperature. Both shear and extensional viscosity of the extruded melt reveal typical thinning behavior and decreases with the increase of melt temperature within the shear rate range *ca.* 10^2-10^3 s^{-1}. Morphological comparison results show that well controlled bead shape can be obtained when the feeding and rastering process are consistent and stable. A lower nozzle height favors increased packing density and reduces internal voids of printed part, leading to enhanced tensile property. The stacking morphology of deposited bead affects the dependence of tensile performance on the porosity and bead cross-section profile. In order to obtain an insight of the tensile property dependence, two bonded adjacent beads with three contacting models show apparently different releasing stress-strain behavior. A large nozzle height leads to loss of control of bead shape and deterioration of the interfacial contact morphology; however, the squeezing effect occurring at a low nozzle height promotes mutual molecular diffusion and

consequently improves the bonding strength. Such interfacial bonding strength is also related to the interfacial contacting area, which is dependent on the bead profile.

5. Acknowledgements

The support provided by China Scholarship Council (CSC) during the academic visit of author Xiang Lin to University of Bradford is acknowledged (NO. FF).

References

[1] D. Popescu, A. Zapciu, C. Amza, F. Baciu, R. Marinescu, FDM process parameters influence over the mechanical properties of polymer specimens: A review, Polym. Test.69 (2018)157-166.

[2] D. J. Horst, C. A. Duvoisin, R. de Almeida Vieira, Additive Manufacturing at Industry 4.0: a Review, Int. J. Eng. Tech. Res. 8 (2018) 3-8.

[3] X. Wang, M. Jiang, Z. Zhou, J. Gou, D. Hui, 3D printing of polymer matrix composites: a review and prospective, Compos. Part B-Eng.110 (2017) 442-458.

[4] B. P. Conner, G. P. Manogharan, A. N. Martof, L. M. Rodomsky, C. M. Rodomsky, D. C. Jordan, J. W. Limperos, Making sense of 3D printing: Creating a map of additive manufacturing products and services, Addit. Manuf. 1-4 (2014) 64-76.

[5] S. Ford, M. Despeisse, Additive manufacturing and sustainability: an exploratory study of the advantages and challenges, J. Clean. Prod. 137 (2016) 1573-1587.

[6] C.W. Hull, Apparatus for production of three-dimensional objects by stereolithography, 1986, Patent Number: 4,575,330.

[7] J.Y. Lee, A. Jia, C.K. Chua, Fundamentals and applications of 3D printing for novel materials, Appl. Mater. Today 7 (2017) 120-133.

[8] C. Yang, X. Tian, D. Li, Y. Cao, F. Zhao, C. Shi, Influence of thermal processing conditions in 3D printing on the crystallinity and mechanical properties of PEEK material, J. Mater. Process. Tech. 248 (2017) 1-7.

[9] F. Ning, W. Cong, J. Qiu, J. Wei, S. Wang, Additive manufacturing of carbon fiber reinforced thermoplastic

composites using fused deposition modeling, Compos. Part B-Eng. 110 (2017) 442-458.

[10] G. Postiglione, G. Natale, G. Griffini, M. Levi, S. Turri, Conductive 3D microstructures by direct 3D printing of polymer/carbon nanotube nanocomposites via liquid deposition modeling, Compos. Part A-Appl. Sci. Manuf. 76 (2015) 110-114.

[11] K. Gnanasekaran, T. Heijmans, S. van Bennekom, H. Woldhuis, S. Wijnia, G. de With, H. Friedrich, 3D printing of CNT- and graphene-based conductive polymer nanocomposites by fused deposition modeling, Appl. Mater. Today 9 (2017) 21-28.

[12] E. A. Papon, A. Haque, Fracture toughness of additively manufactured carbon fiber reinforced composites, Addit. Manuf. 26 (2019) 41-52.

[13] A. de Leon, Q. Chen, N. Palaganas, J. Palaganas, J. Manapat, R. Advincula, High performance polymer nanocomposites for additive manufacturing applications, React. Funct. Polym. 103 (2016)141–155.

[14] Q. Chen, P. F. Cao, R. C. Advincula, Mechanically robust, ultraelastic hierarchical foam with tunable properties via 3D printing, Adv. Funct. Mater. 28 (2018) 1800631.

[15] J. R. C. Dizon, A. H. Espera, Q. Chen, R. C. Advincula, Mechanical characterization of 3D-printed polymers, Addit. Manuf. 20 (2018) 44-67.

[16] D. Kazmer, 28-Three-dimensional printing of plastics, applied plastics engineering handbook, 2nd ed., Lowell Ma, United States, 2017, pp. 617-634.

[17] M. Monzón, Z. Ortega, A. Martínez, F. Ortega, Standardization in additive manufacturing: activities carried out by international organizations and projects, Int. J. Adv. Manuf. Technol. 76 (2015) 1111-1121.

[18] A. Forster, Materials testing standards for additive manufacturing of polymer materials, National Institute of Standards and Technology Interagency Report 8059, Department of Commerce, 2015.

[19] J. Stampfl, M. Schuster, S. Baudis, H. Lichtenegger, R. Liska, Biodegradable stereolithography resins with defined mechanical properties, Virtual Rapid Manuf. Proc. VRAP (2007) 283–288

[20] J. Manapat, J. Mangadlao, B. Tiu, G. Tritchler, R. Advincula, High-strength stereolithographic 3D printed nanocomposites: graphene oxide metastability, ACS Appl. Mater. Interfaces 9 (1) (2017) 10085-10093.

[21] B. Rankouhi, S. Javadpour, F. Delfanian, T. Letcher, Failure analysis and mechanical characterization of 3D printed ABS with respect to layer thickness and orientation, J. Fail. Anal. Prev. 16 (3) (2016) 467-481.

[22] S. Guessasma, S. Belhabib, H. Nouri, O. Hassana, Anisotropic damage inferred to 3D printed polymers using fused deposition modelling and subject to severe compression, Eur. Polym. J. 85 (2016) 324-340.

[23] S.H. Ahn, M. Montero, D. Odell, S. Roundy, P. K. Wright, Anisotropic material properties of fused deposition modelling ABS, Rapid Prototyp. J. 8(4) (2002) 248-57.

[24] C. Wendt, M. Batista, E. Moreno, A. Valerga, S. Fernández-Vidal, O. Droste, M. Marcos, Preliminary design and analysis of tensile test samples developed by additive manufacturing, Procedia Eng. 132 (2015) 132-139.

[25] T. Letcher, B. Rankouhi, S. Javadpour, Experimental study of mechanical properties of additively manufactured ABS plastic as a function of layer parameters, in: Proceedings of the ASME 2015 International Mechanical Engineering Congress and Exposition IMECE2015, Houston, 2015

[26] Q. Sun, G. M. Rizvi, C. T. Bellehumeur, P. Gu, Effect of processing conditions on the bonding quality of FDM polymer filaments. Rapid Prototyp. J. 14(2) (2008) 72-80.

[27] D. Türk, F. Brenni, M. Zogg, M. Meboldt, Mechanical characterization of 3D printed polymers for fiber reinforced polymers processing, Mater. Des. 118 (2017) 256-265.

[28] T. Letcher, M. Waytashek, Material property testing of 3D-printed specimen in PLA on an entry-level 3D printer, in: Proceedings of the ASME 2014International Mechanical Engineering Congress & Exposition (IMECE2014), Montreal, 2014.

[29] S. A. Tronvoll, T. Welo, C. W. Elverum, The effects of voids on structural properties of fused deposition modeled parts: a probabilistic approach. Inter. J. Adv. Manuf. Technol. 97 (2018) 3607-3618.

[30] O. S. Es-Said, J. Foyos, R. Noorani, M. Mandelson, R. Marloth, B. A. Pregger, Effect of layer orientation on mechanical properties of rapid prototyped samples, Mater. Manuf. Process. 15(1) (2000) 107-22.

[31] S. Maidin, J. H. U. Wong, A. S. Mohamed, S. B. Mohamed, Effect of vacuum assisted fused deposition modeling on 3D printed ABS microstructure, Inter. J. Appl. Eng. Res. 12(15) (2017) 4877-4881.

[32] B. Vasudevarao, D. P. Natarajan, A. Razdan, H. Mark, Sensitivity of RP surface finish to process parameter variation. In: Proceedings of solid free form fabrication. Austin, USA; 2000. pp. 252-258.

[33] S. B. Balani, F. Chabert, V. Nassiet, A. Cantarel, Influence of printing parameters on the stability of deposited beads in fused filament fabrication of poly (lactic) acid, Addit. Manuf. 25 (2019) 112-121.

[34] A. Sood, R. Ohdar, S. Mahapatra, Parametric appraisal of mechanical property of fused deposition modelling processed parts, Mater. Des. 31 (2010) 287-295.

[35] L.G. Blok, M.L. Longana, H. Yu, B.K.S. Woods, An investigation into 3D printing of fiber reinforced thermoplastic composites, Addit. Manuf. 22 (2018) 176-186.

[36] S. Dadbakhsh, L. Verbelen, T. Vandeputte, D. Strobe, P. Puyvelde, J. Kruth, Effect of powder size and shape on the SLS processability and mechanical properties of a TPU elastomer, Phys. Procedia 83 (2016) 971-980.

[37] S. Ziegelmeier, P. Christou, F. Wöllecke, C. Tuck, R. Goodridge, R. Hague, E. Krampe, E. Wintermantel, An experimental study into the effects of bulk and flow behaviour of laser sintering polymer powders on resulting part properties, J. Mater. Process. Tech. 215(1) (2015) 239-250.

[38] S. Yuan, F. Shen, J. Bai, C. K. Chua, J. Wei, K. Zhou, 3D soft auxetic lattice structures fabricated by selective laser sintering: TPU powder evaluation and process optimization, Mater. Design 120 (2017) 317-327.

[39] F. Norazman, N. Hopkinson, Effect of sintering parameters and flow agent on the mechanical properties of high speed sintered elastomer, J. Manuf. Sci. Eng.136 (2014) 061006.

[40] L. Verbelen, S. Dadbakhsh, V. D. E. Michael, D. Strobbe, J. P. Kruth, B. Goderis, P. Van Puyvelde, Analysis of the material properties involved in laser sintering of thermoplastic polyurethane, Addit. Manuf. 15 (2017) 12-19.

[41] M. A. León-Cabezas, A. Martínez-García, F. J. Varela-Gandía, Innovative functionalized monofilaments for 3D printing using fused deposition modeling for the toy industry. Procedia Manuf. 13 (2017) 738-745.

[42] A. Haryńska, I. Gubanska, J. Kucinska-Lipka, H. Janik, Fabrication and characterization of flexible medical-grade TPU filament for fused deposition modeling 3DP technology, Polymers 10 (2018) 1304.

[43] J. F. Christ, N. Aliheidari, A. Ameli, P. Pötschke, 3D printed highly elastic strain sensors of multiwalled carbon nanotube/thermoplastic polyurethane nanocomposites, Mater. Design 131 (2017) 394-401.

[44] J. F. Christ, N. Aliheidari, P. Pötschke, A. Ameli, Bidirectional and stretchable piezoresistive sensors enabled by multimaterial 3D printing of carbon nanotube/thermoplastic polyurethane nanocomposites, Polymers 11(1) (2018) 11.

[45] K. Kim, J. Park, J. Suh, M. Kim, Y. Jeong, I. Park, 3D printing of multiaxial force sensors using carbon nanotube(CNT)/thermoplastic polyurethane (TPU) filaments, Sensor. Actuat. A-Phys. 263 (2017) 493-500.

[46] J. Z. Gul, M. Sajid, M. M. Rehman, G. U. Siddiqui, I. Shah, K. Y. Kim, J. W. Lee, K. H. Choi, 3D printing for soft robotics – a review. Sci. Technol. Adv. Mater. 19(1) (2018) 243-262.

[47] X. Kuang, K. Chen, C. K. Dunn, J. Wu, V. C. F. Li, H. J. Qi, 3D printing of highly stretchable, shape-memory, and self-healing elastomer toward novel 4D printing, ACS Appl. Mater. Interfaces 10 (2018) 7381-7388.

[48] B. Huang, S. Singamneni, Raster angle mechanics in fused deposition modelling, J. Compos. Mater. 49(3) (2014) 1-21.

[49] R. Comminal, M. P. Serdeczny, D. B. Pedersen, J. Spangenberg, Numerical modeling of the strand deposition flow in extrusion-based additive manufacturing, Addit. Manuf. 20 (2018) 68-76.

[50] M. P. Serdeczny, R. Comminal, D. B. Pedersen, J. Spangenberg, Experimental validation of a numerical model for the strand shape in material extrusion additive manufacturing, Addit. Manuf. 24 (2018) 145-153.

[51] M. Hebda, C. McIlroy, B. Whiteside, F. Caton-Rose, P. Coates. A method for predicting geometric characteristics of polymer deposition during fused-filament-fabrication. Addit. Manuf. 27 (2019) 99-108.

[52] N. Aliheidari, R. Tripuraneni, A. Ameli, S. Nadimpalli, Fracture resistance measurement of fused deposition modeling 3D printed polymers, Polym. Test. 60 (2017) 94-101.

[53] M. Rafailovich, Y. Shmueli, J. Jiang, Y. Zhou, G. Yuan, S. Satija, S. Lee, T. Kim, G. Marom, D. Gersappe, In-situ X-ray and thermal imaging of 3D printed PLA, Bulletin of the American Physical Society, March 2019, Boston, USA

[54] O. Pokluda, C. T. Bellehumeur, J. Vlachopoulos, Modification of Frenkel's model for sintering, AIChE J. 43 (1997) 3253-3256.

[55] H. Zhang, K. Lamnawar, A. Maazouz, Rheological modeling of the diffusion process and the interphase of symmetrical bilayers based on PVDF and PMMA with varying molecular weights. Rheol. Acta. 51 (2012) 691-711.

Appendix A

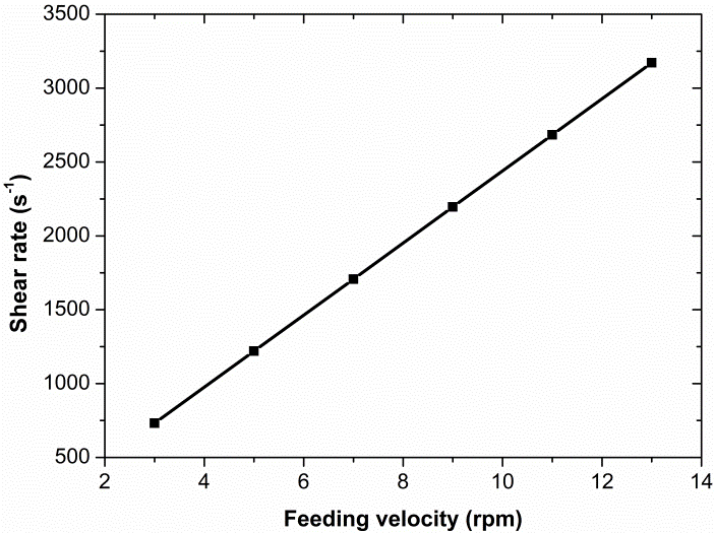

Fig. A.1 The relationship of gear feeding velocity (revolution speed) *vs.* apparent shear rate

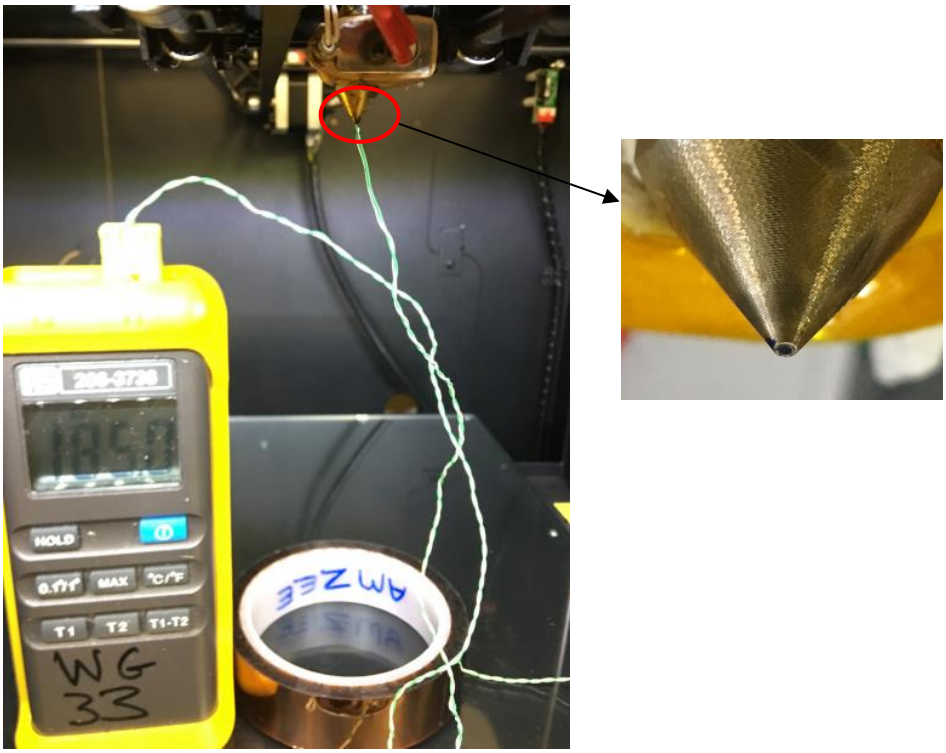

Fig. A.2 Nozzle tip and the measurement of actual nozzle temperature

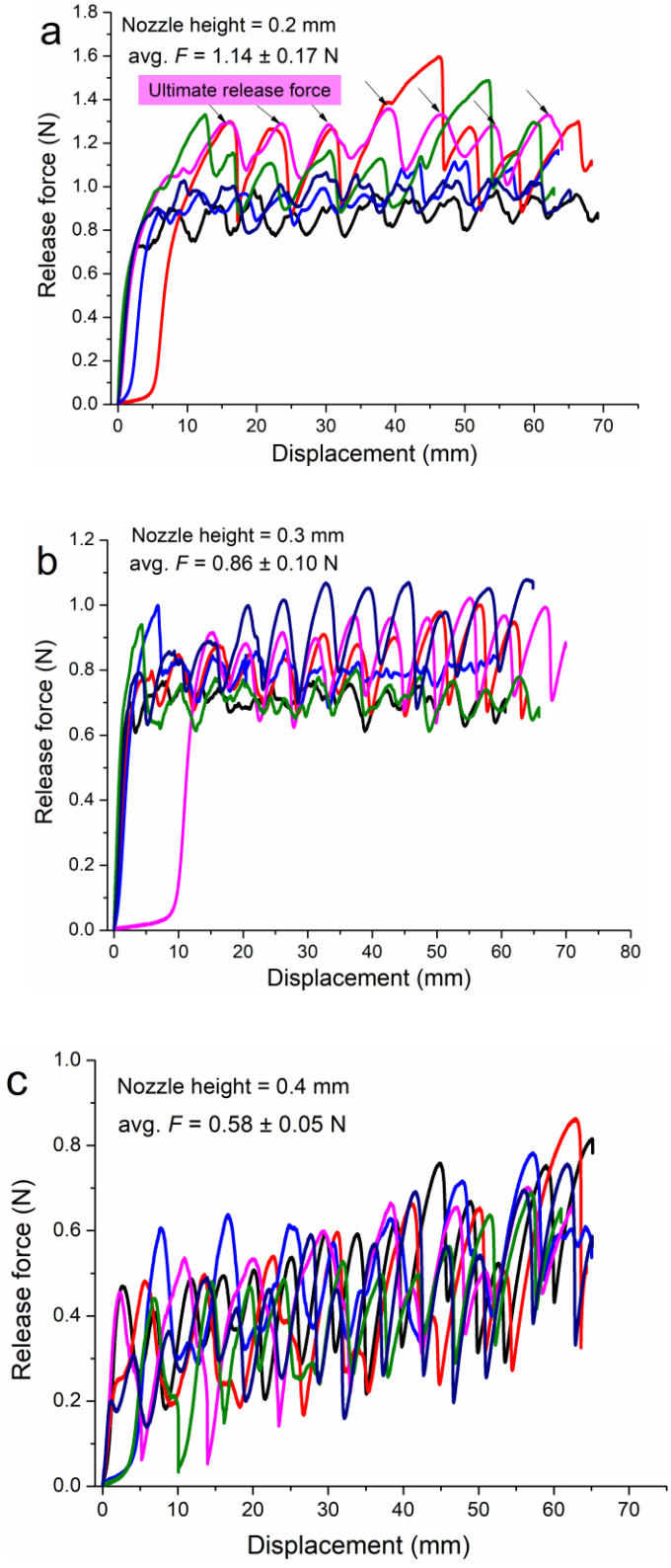

Fig. A.3 Release behavior of bonded beads measured under displacement controlled conditions at a constant cross head speed of 0.5 mm/s for h=0.2, 0.3 and 0.4 mm, respectively. The release force curves demonstrated as sinusoidal fluctuation and the peak values (the pink curve marked by arrows in Fig. A. 3a) was used as the onset of release. Each model was tested for six times.

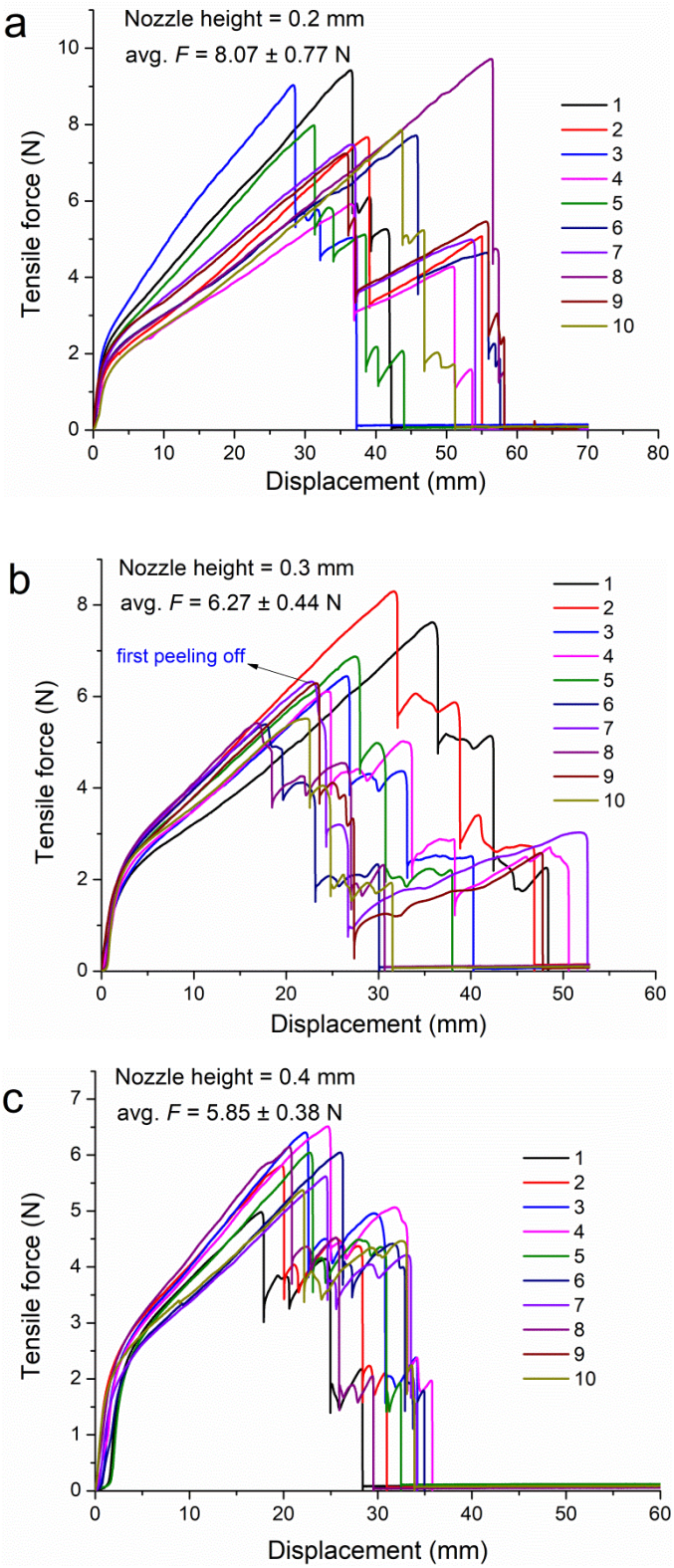

Fig. A.4 Tensile behavior of bonded beads measured under displacement controlled conditions at a constant cross head speed of 0.5 mm/s for h=0.2, 0.3 and 0.4 mm, respectively. Herein, ten samples for each model were tested. Similarly, the first yield peak point in the tensile curves was regarded as the critical value of the onset of delamination.